



Published in final edited form as:

*Abdom Radiol (NY)*. 2016 May ; 41(5): 946–953. doi:10.1007/s00261-016-0659-1.

## Restriction spectrum imaging improves MRI-based prostate cancer detection

Kevin C. McCammack<sup>1</sup>, Natalie M. Schenker-Ahmed<sup>1</sup>, Nathan S. White<sup>1</sup>, Shaun R. Best<sup>1</sup>, Robert M. Marks<sup>2</sup>, Jared Heimbigner<sup>2</sup>, Christopher J. Kane<sup>3</sup>, J. Kellogg Parsons<sup>3</sup>, Joshua M. Kuperman<sup>1</sup>, Hauke Bartsch<sup>1</sup>, Rahul S. Desikan<sup>1</sup>, Rebecca A. Rakow-Penner<sup>1</sup>, Michael A. Liss<sup>4</sup>, Daniel J. A. Margolis<sup>5</sup>, Steven S. Raman<sup>5</sup>, Ahmed Shabaik<sup>6</sup>, Anders M. Dale<sup>1,7</sup>, and David S. Karow<sup>1</sup>

<sup>1</sup>Department of Radiology, University of California San Diego School of Medicine, 200 W Arbor Dr, San Diego, CA 92103, USA

<sup>2</sup>Department of Radiology, Naval Medical Center San Diego, San Diego, USA

<sup>3</sup>Department of Urology, University of California San Diego School of Medicine, San Diego, USA

<sup>4</sup>Department of Urology, University of Texas San Antonio School of Medicine, San Antonio, USA

<sup>5</sup>Department of Radiology, University of California Los Angeles Geffen School of Medicine, Los Angeles, USA

<sup>6</sup>Department of Pathology, University of California San Diego School of Medicine, San Diego, USA

<sup>7</sup>Department of Neurosciences, University of California San Diego School of Medicine, San Diego, USA

### Abstract

**Purpose**—To compare the diagnostic performance of restriction spectrum imaging (RSI), with that of conventional multi-parametric (MP) magnetic resonance imaging (MRI) for prostate cancer (PCa) detection in a blinded reader-based format.

---

Correspondence to: David S. Karow; *email*: dkarow@ucsd.edu.

**Electronic supplementary material** The online version of this article (doi:10.1007/s00261-016-0659-1) contains supplementary material, which is available to authorized users.

**Conflict of Interest** All authors declared that they have no conflict of interest.

**Disclaimer** The views expressed in this presentation are those of the authors and do not necessarily reflect the official policy or position of the Department of the Navy, Department of Defense, or the United States Government. The authors are military service members. This work was prepared as part of official duties. Title 17 U.S.C. 105 provides that ‘Copyright protection under this title is not available for any work of the United States Government.’

**Ethical Approval** All procedures performed in studies involving human participants were in accordance with the ethical standards of the institutional and/or national research committee and with the 1964 Helsinki declaration and its later amendments or comparable ethical standards.

**Informed Consent** Signed informed consent was waived by our Institutional Review Board as RSI has been integrated into the standard prostate MRI workflow at our institution as a diffusion tensor imaging product sequence-based technique with multiple *b* values, anteroposterior/posteroanterior distortion correction, and unique post-processing.

**Methods**—Three readers independently evaluated 100 patients (67 with proven PCa) who underwent MP-MRI and RSI within 6 months of systematic biopsy ( $N = 67$ ; 23 with targeting performed) or prostatectomy ( $N = 33$ ). Imaging was performed at 3 Tesla using a phased-array coil. Readers used a five-point scale estimating the likelihood of PCa present in each prostate sextant. Evaluation was performed in two separate sessions, first using conventional MP-MRI alone then immediately with MP-MRI and RSI in the same session. Four weeks later, another scoring session used RSI and T2-weighted imaging (T2WI) without conventional diffusion-weighted or dynamic contrast-enhanced imaging. Reader interpretations were then compared to prostatectomy data or biopsy results. Receiver operating characteristic curves were performed, with area under the curve (AUC) used to compare across groups.

**Results**—MP-MRI with RSI achieved higher AUCs compared to MP-MRI alone for identifying high-grade (Gleason score greater than or equal to  $4 + 3 = 7$ ) PCa (0.78 vs. 0.70 at the sextant level;  $P < 0.001$  and 0.85 vs. 0.79 at the hemigland level;  $P = 0.04$ ). RSI and T2WI alone achieved AUCs similar to MP-MRI for high-grade PCa (0.71 vs. 0.70 at the sextant level). With hemigland analysis, high-grade disease results were similar when comparing RSI + T2WI with MP-MRI, although with greater AUCs compared to the sextant analysis (0.80 vs. 0.79).

**Conclusion**—Including RSI with MP-MRI improves PCa detection compared to MP-MRI alone, and RSI with T2WI achieves similar PCa detection as MP-MRI.

### Keywords

Prostate MRI; Prostate cancer; Diffuse weighted imaging; Restriction spectrum imaging; Prostate diffusion imaging

---

Prostate cancer (PCa) is the most commonly diagnosed noncutaneous malignancy and second leading cause of cancer death for men in the United States [1]. Magnetic resonance imaging (MRI) has proven useful for PCa detection, localization, and staging, and most recently has demonstrated value for guiding prostate biopsy when fused with ultrasound [2–5]. Conventional multi-parametric (MP) MRI, including diffusion-weighted imaging (DWI), dynamic contrast enhancement (DCE), and standard anatomic imaging consisting of T1-weighted (T1WI) and T2-weighted imaging (T2WI) has produced the most consistent results to date and serves as the standard-of-care for in situ PCa imaging [2, 3, 6, 7]. However, improved PCa detection by MRI is the goal of considerable ongoing effort.

Conventional DWI is arguably the most important contributor of the individual MP-MRI components for PCa detection, outperforming standard anatomic imaging, and DCE methodologies [3, 7–12]. Diffusion techniques are particularly attractive because they are rapid and utilize inherent tissue contrast properties, not requiring intravenous gadolinium agents with their associated risk, cost, and inconvenience. However, conventional DWI is limited in many contexts commonly encountered in the prostate, including hemorrhage, infection, and inflammation. An additional significant limitation of conventional DWI is its frequent degradation by marked spatial distortion [13]. Improvements in DWI technique may substantially improve the clinical utility of PCa imaging.

Restriction spectrum imaging (RSI) [14] is an innovative, advanced diffusion sequence that aims to improve upon the strengths and address the shortcomings of conventional DWI in

oncologic imaging [15, 16]. It uses the data obtained from an extended range of multiple  $b$  value, multidirectional diffusion images to model a distribution, or spectrum of isotropic and anisotropic water compartments in tissue. The spectrum parameters can then be used to isolate the signal contribution from intracellular restricted water molecules, while attenuating the signal contribution from the extracellular hindered and free water pools which typically confound conventional DWI [14–17]. The goal is improved conspicuity of highly cellular tumors, which has proven effective in the brain [16–19] and more recently the prostate, though these prior studies were limited by design which involved placement of regions of interest based on knowledge of tumor location [20, 21]. RSI additionally corrects for spatial distortion through acquiring  $b = 0$  images with both forward and reverse phase encoding polarities, and corrects for Eddy currents, allowing for more precise tumor localization and useful in the identification of extraprostatic extension of PCa [20, 22, 23].

In this study, we investigated the clinical efficacy of RSI for PCa detection, comparing it directly to current standard-of-care MP-MRI in a blinded reader-based format, which most accurately reflects the current practice model in most centers, to evaluate for true clinical utility of the technique.

## Methods

### Patients

Institutional review board approval was obtained for this retrospective study, with signed patient consent waived as RSI has been integrated into the standard prostate MRI workflow at our institution as a diffusion tensor imaging product sequence-based technique with multiple  $b$  values, anteroposterior/posteroanterior distortion correction, and unique post-processing. We evaluated 111 patients with imaging consisting of MP-MRI with RSI performed within 6 months of either radical prostatectomy with whole mount pathology or systematic biopsy. The indications for MP-MRI in this patient population are summarized in Table 1. Forty-five patients had already had prior biopsy performed, with 40 returning results positive for PCa. Required pulse sequences included T1WI, T2WI, DCE, DWI (including ADC maps), and RSI. Eleven patients were excluded from the study due to lack of an available ADC map for the evaluation (Fig. 1).

### MRI acquisition

All studies were performed on a 3.0-T GE Signa HDxt scanner (GE Medical Systems, Milwaukee, WI) using a cardiac surface coil but without an endorectal coil. Glucagon is not administered at our center to decrease rectal peristalsis and no bowel preparation is performed. The entire prostate is imaged, with axial slices oriented perpendicular to the rectal wall. The following conventional sequences were obtained: axial and coronal T2WI, axial T1WI, axial free-breathing DWI ( $b$  values of 0 and 1000 s/mm<sup>2</sup>), and axial free-breathing DCE performed before, during, and after single-dose injection of approximately 20 mL gadobenate dimeglumine (Multihance, Bracco Imaging, Milan, Italy). DCE is performed with 32 output temporal phases at approximately 8 s per phase for a total scan time of approximately 4 min with no injection delay.

RSI was performed using spin echo, echo planar imaging at  $b$  values of 0, 125, 375, and 1000  $\text{s/mm}^2$  with 6, 6, and 15 directions at each respective nonzero  $b$  value. The  $b = 0$   $\text{s/mm}^2$  images were performed with phase encoding in both the forward and reverse directions to correct for spatial distortion due to magnetic field inhomogeneity. The sequence takes approximately 5 min to perform on the HDxt system. RSI cellularity maps (CMs) were derived using the signal fraction of the restricted isotropic component of the diffusion spectrum [16] and coregistered to axial T2WI images (Fig. 2). RSI-CMs were reconstructed using data from all  $b$  values, which were then standardized across all patients to obtain RSI-MRI  $z$  score maps. RSI  $z$  score maps were calculated by (1) measuring the mean and standard deviation of normal prostate signal from the raw RSI-CM data of a representative normal population (three normal subjects, as determined by radiologist interpretation (DSK), which were separate from the current study population), (2) subtracting the measured mean value from each subject's CM, and (3) dividing the result by the standard deviation of measured normal prostate. Additional specific sequence parameters are summarized in Table 2.

### Image interpretation

Three radiologists (SRB, a body imaging fellow with dedicated interest in prostate imaging and over 1 year of experience interpreting prostate MRI; JH, a body imaging fellowship-trained attending radiologist with over 2 years of experience interpreting prostate MRI; RMM, a body imaging fellowship-trained attending radiologist with over 3 years of experience interpreting prostate MRI) who were each blinded to clinical and laboratory data evaluated MRI cases independently. Overall, three different sets of imaging data were evaluated in two sessions. During the initial session, cases were first scored using just MP-MRI (consisting of T1WI and T2WI, DWI with ADC, and DCE), then immediately thereafter scored again using RSI in addition to MP-MRI. After a 4 week wash-out period, the cases were then scored using just RSI and T2WI. Readers were instructed to interpret RSI-CMs as suspicious for PCa when focal/asymmetrically increased signal was identified in the PZ, or within the TZ in areas not clearly corresponding to benign prostatic hyperplasia nodules as suggested by the presence of a hypointense capsule on T2WI. The sextant model was utilized (right and left base, midgland, and apex), with a 5-point Likert scale assigned for each sextant (1, definitely absent; 2, probably absent; 3, indeterminate; 4, probably present; and 5, definitely present). For the purposes of subsequent statistical analyses, reader scores of 4 and 5 were considered positive for PCa by imaging as per precedent established by prior similarly structured studies [7, 24]. Prostate Imaging and Data Reporting System version 2 (PIRADSv2) was not employed.

### Reference standard

Thirty-three patients underwent prostatectomy. After prostatectomy, each specimen was fixed in 10% neutral-buffered formalin and then embedded in paraffin. Whole mount histopathology was performed on 4- $\mu\text{m}$ -thick sections stained with hematoxylin and eosin (H&E). A board-certified anatomic pathologist with over 24 years of prostate expertise evaluated the pathology, outlining the boundaries of each tumor and assigning a Gleason score (GS) to each identified tumor.

Biopsy results were used as the reference standard in 67 patients. Twelve cores are routinely performed at our institution via the extended sextant model, and are then interpreted by experienced genitourinary pathologists, assigning GS to each core as well as a percentage core involvement with PCa, when present. While biopsy targeting planning served as the study indication for 11 of our patients, overall biopsy targeting was performed in 23 patients for whom biopsy served as the reference standard. Otherwise, systematic biopsy core locations were defined by the urologist at the time of sampling, and were unable to be definitively correlated with MRI imaging.

For this evaluation, distinction was made between high and low/intermediate grade cancer, as per precedent established by prior Standards of Reporting for MRI-targeted Biopsy Studies working group recommendations [4, 5, 25]. Specifically, GS greater than or equal to 4 + 3=7 was considered as high grade.

### Statistical analysis

Receiver operating characteristic (ROC) curves were created using maximum-likelihood estimation for each reader and each of the three imaging sets. Analysis was first performed on the sextant level overall, and then using the prostatectomy cases alone. Additionally, because one-to-one matching was not performed for the whole mount pathology, and because prostate midgland definition can vary from practitioner to practitioner, a sidedness evaluation was undertaken to maximize the PCa detection rate. Area under the ROC curve (AUC) was used as a general indicator of quality and compared across data sets using the nonparametric method proposed by Obuchowski [26]. Comprehensive comparisons were made by covarying for reader. Sensitivity, specificity, positive predictive value, and negative predictive value on the sextant level were calculated. For all tests, *P* values of <0.05 were denoted as statistical significance.

Inter-reader agreement analysis was performed using kappa statistics with quadratic weights. Cohen's Kappa was performed to evaluate agreement between any two readers, while the adapted Fleiss Kappa was used to assess agreement between all three readers simultaneously. Kappa values of 0–0.20 denoted slight agreement, 0.21–0.40 fair agreement, 0.41–0.60 moderate agreement, 0.61–0.80 substantial agreement, and 0.81–1 almost perfect agreement [27].

All statistical analyses were performed using R version 3.1.2 software (The R Foundation for Statistical Computing, Vienna, Austria).

## Results

### Histopathology

PCa was present in 67 of 100 patients (67%) and 176 of 600 sextants (29%). High-grade PCa specifically was identified in 30 of 100 patients (30%) and 88 of 600 sextants (15%). Additional GS information as well as clinical data are summarized in Table 3. Representative cases of imaging with subsequent histopathology are demonstrated in Fig. 3.

## Diagnostic performance

For the identification of all PCa as well as specifically high-grade PCa, MP-MRI in combination with RSI produced superior performance (Table 4). On the sextant level, MP-MRI with RSI produced a combined AUC of 0.66 for all PCa and 0.78 for specifically high-grade PCa. This improved capability of MP-MRI plus RSI over MP-MRI alone was statistically significant for all three readers for all PCa ( $P < 0.001$ ) and specifically high-grade PCa ( $P < 0.001$ ). Hemigland analysis produced similar results, with superior performance of MP-MRI plus RSI relative to MP-MRI alone for all PCa ( $P = 0.001$ ) and specifically high-grade PCa (AUC of 0.85 vs. 0.79;  $P = 0.04$ ).

RSI and T2WI alone on the sextant level produced statistically equivalent performance to MP-MRI for readers 1 and 3 for both all PCa and high-grade PCa. For reader 2, RSI and T2WI outperformed MP-MRI on the sextant level ( $P < 0.001$  for all PCa and  $P = 0.03$  for high-grade PCa) (Table 4). Hemigland analysis demonstrates similar AUCs when comparing RSI and T2WI with MP-MRI (e.g., AUCs of 0.80 vs. 0.79;  $P = 0.77$  for high-grade disease), with reader 2 trending toward superior performance using RSI + T2WI (Table 4).

Sensitivity, specificity, positive and negative predictive value figures on the sextant basis are listed in the supplementary Table.

## Inter-reader agreement

By accepted criteria, there was moderate agreement for all imaging protocols for all comparisons between any two readers as well as between all three simultaneously [27]. There was a trend toward increased inter-reader agreement with incorporation of RSI, with the greatest agreement utilizing RSI and T2WI alone. Between readers 1 and 2, actually there was substantial agreement with RSI and T2WI alone, the only comparison to reach that level within this data set (Table 5).

## Discussion

Our data indicate that RSI combined with MP-MRI improves PCa detection, and that RSI + T2WI may perform similarly to or better than MP-MRI. Additionally, our study suggests that RSI may promote greater consensus in reader interpretation, with inter-reader agreement increasing when RSI is combined with MP-MRI and most uniform when readers use RSI alone, though admittedly the effect was modest in this study.

Prior studies have supported the importance of diffusion techniques, particularly conventional DWI, in MP-MRI for PCa detection, and localization [3, 7–12]. With more robust gradient performance made possible by improved scanner technologies, advanced diffusion techniques have been devised and methodologies such as diffusion kurtosis imaging have been evaluated for PCa identification with mixed results to date [28–30]. RSI is an advanced diffusion technique that employs multiple  $b$  values and multiple directions to focus recorded signal from the isotropic, truly restricted pool of water molecules in tissue. RSI can be acquired on any 3 Tesla imaging platform and the post-processing performed on any independent workstation via readily available post-processing software. The goal is improved conspicuity of cellular lesions, originally devised for the evaluation of brain

tumors [16–19], and applied more recently with promise in the prostate [20, 21]. This study is the first reader-based evaluation of RSI for PCa detection and localization.

RSI may provide a viable diagnostic MRI option to those patients for whom MP-MRI is not possible, most notably those with contraindications to intravenous contrast material due to renal insufficiency or allergy, or those unable to tolerate prolonged scan times. The sequence is achieved without the need for any intravenous gadolinium administration and requires only up to 5 min depending on scanner type and gradient performance. These data also raise the possibility of evaluating RSI + T2WI in isolation as a short, targeted screening exam in at risk individuals. Our data suggest these patients will have the benefit of comparable reader interpretation performance using RSI as those with the more exhaustive MP-MRI.

Reader interpretations also demonstrated less variability when RSI was incorporated with MP-MRI, and inter-reader agreement was in fact the highest when RSI was evaluated in isolation. This suggests that in addition to the improved PCa detection allowed by RSI, it also provides greater consistency between readers perhaps through relative ease of interpretation. MP-MRI involves numerous sequences and its interpretation is relatively labor intensive; it is possible that through processing these data involved, readers become more prone to variability in their analyses. RSI color maps are simply overlaid on T2WI and require much less reader effort due to the clarity and relative paucity of images compared to MP-MRI, at a comparable rate of performance.

Prior reader-based evaluations of current standard-of-care MP-MRI for PCa detection demonstrate AUC figures ranging from as low as 0.67 to as high as 0.90 [6, 7, 31]. Our results fall within this range, albeit toward the lower end. This may be due to the fact that our cases represent predominantly low-grade PCa, which is known to be detected less accurately than high-grade PCa by MRI [24]. Additionally, approximately two-thirds of our cases utilized biopsy results as the tissue standard which would be expected to adversely impact our calculations due to known inaccuracies associated with biopsy compared to prostatectomy [32–34]. Further, one-to-one matching between imaging, biopsy, and prostatectomy was not performed, which may allow variations in anatomic definition between practitioners to adversely affect our figures. Specifically, while definitions of apex, midgland, and base may differ between imaging interpretation, biopsy location definition based on ultrasound, and pathologic evaluation of prostatectomy specimens, sidedness would be expected to remain constant. Hemigland analysis performed to address this possibility did in fact increase our AUC calculations more toward published numbers [6, 7, 31]. Lastly, our readers are at the early stages of their careers, with a maximum of 3 years of dedicated experience, whereas prior studies utilized more senior readers [6, 7, 31]. While this may adversely impact our AUC calculations, the demonstrated efficacy of RSI in relatively naïve readers may actually serve as a study strength, supporting the generalizability of this technique to a wide audience. It is important to note, however, that this study was not designed to compare with prior published AUC data, but rather to directly compare the performance of RSI to MP-MRI. We contend the above factors are effectively controlled for across the different imaging protocols in this study, as the same tissue standard and readers were used throughout. Further, the same trends hold with the data stratified between patients with biopsy results vs. those with whole mount pathology.

Our study has possible limitations in addition to those already discussed above. First, we did not differentiate between PZ and TZ PCa in this study as systematic biopsies at our institution do not routinely differentiate between these regions. Given that two-thirds of our cases relied upon biopsy tissue for analysis, we were limited in our ability to distinguish between PZ and TZ PCa in this population. It would be useful to evaluate the performance characteristics of RSI relative to MP-MRI in both the PZ and TZ in the future. TZ PCa imaging is a known challenge confronting MP-MRI, and we would expect RSI to perform well in comparison due to its decreased vulnerability to background tissue heterogeneity by theoretically focusing on signal arising from within cells themselves. Second, due to the retrospective study design, there was some inevitable variation between MRI and the acquisition of the tissue standard for comparison that could likely be minimized in a prospective design. Given the indolent progression of PCa, this is likely of minimal impact. Finally, no cost analysis was performed to evaluate the impact of implementation of this technology.

In summary, RSI shows promise for PCa detection and localization, statistically improving the ability of readers to localize disease when used in combination with MP-MRI. Further, RSI and T2WI in isolation allows performance comparable to MP-MRI, which may allow adequate imaging in patients unable to receive intravenous contrast material, those unable to tolerate long imaging times, or as a potential surrogate for MP-MRI in specific clinical situations.

## Supplementary Material

Refer to Web version on PubMed Central for supplementary material.

## Acknowledgments

This study was supported by NIH Grant R01EB000790, American Cancer Society, Institutional Research Grant Number 70-002, Department of Defense Prostate Cancer Research Program, Idea Development Award W81XWH-13-1-0391#PC120532, National Science Foundation Grant Number 1430082, and General Electric Investigator Initiated Research Award BOK92325.

*Funding* The authors were funded by R01EB000790, American Cancer Society, Institutional Research Grant Number 70-002; DoD, Prostate Cancer Research Program; Idea Development Award W81XWH-13-1-0391, #PC120532; National Science Foundation, Grant Number 1430082; UCSD Clinician Scientist Program; and General Electric, Investigator Initiated Research Award BOK92325.

## References

1. American Cancer Society. Cancer facts and figures. Atlanta: American Cancer Society; 2013.
2. Turkbey B, Pinto PA, Mani H, et al. Prostate cancer: value of multiparametric MR imaging at 3T for detection—histopathologic correlation. *Radiology*. 2010; 255:89–99. [PubMed: 20308447]
3. Isebaert S, Van den Bergh L, Haustermans K, et al. Multiparametric MRI for prostate cancer localization in correlation to whole-mount histopathology. *J Magn Reson Imaging*. 2013; 37:1392–1401. DOI: 10.1002/jmri.23938 [PubMed: 23172614]
4. Siddiqui MM, Rais-Bahrami S, Turkbey B, et al. Comparison of MR/ultrasound fusion-guided biopsy with ultrasound-guided biopsy for the diagnosis of prostate cancer. *JAMA*. 2015; 313:390–397. DOI: 10.1001/jama.2014.17942 [PubMed: 25626035]



5. Siddiqui MM, Rais-Bahrami S, Truong H, et al. Magnetic resonance imaging/ultrasound-fusion biopsy significantly upgrades prostate cancer versus systematic 12-core transrectal ultrasound biopsy. *Eur Urol.* 2013; 64:713–719. DOI: 10.1016/j.eururo.2013.05.059 [PubMed: 23787357]
6. Kitajima K, Kaji Y, Fukabori Y, et al. Prostate cancer detection with 3 T MRI: comparison of diffusion-weighted imaging and dynamic contrast-enhanced MRI in combination with T2-weighted imaging. *J Magn Reson Imaging.* 2010; 31:625–631. DOI: 10.1002/jmri.22075 [PubMed: 20187206]
7. Donati OF, Jung SI, Vargas HA, et al. Multiparametric prostate MR imaging with T2-weighted, diffusion-weighted, and dynamic contrast-enhanced sequences: are all pulse sequences necessary to detect locally recurrent prostate cancer after radiation therapy? *Radiology.* 2013; 268:440–450. DOI: 10.1148/radiol.13122149/-/DC1 [PubMed: 23481164]
8. Tan CH, Wei W, Johnson V, Kundra V. Diffusion-weighted MRI in the detection of prostate cancer: meta-analysis. *AJR Am J Roentgenol.* 2012; 199:822–829. DOI: 10.2214/AJR.11.7805 [PubMed: 22997374]
9. Soylu FN, Peng Y, Jiang Y, et al. Seminal vesicle invasion in prostate cancer: evaluation by using multiparametric endorectal MR imaging. *Radiology.* 2013; 267:797–806. DOI: 10.1148/radiol.13121319/-/DC1 [PubMed: 23440325]
10. Langer DL, van der Kwast TH, Evans AJ, et al. Prostate cancer detection with multi-parametric MRI: logistic regression analysis of quantitative T2, diffusion-weighted imaging, and dynamic contrast-enhanced MRI. *J Magn Reson Imaging.* 2009; 30:327–334. DOI: 10.1002/jmri.21824 [PubMed: 19629981]
11. Peng Y, Jiang Y, Yang C, et al. Quantitative analysis of multiparametric prostate MR images: differentiation between prostate cancer and normal tissue and correlation with Gleason score—a computer-aided diagnosis development study. *Radiology.* 2013; 267:787–796. [PubMed: 23392430]
12. Peng Y, Jiang Y, Antic T, et al. Validation of quantitative analysis of multiparametric prostate MR images for prostate cancer detection and aggressiveness assessment: a cross-imager study. *Radiology.* 2014; 271:461–471. [PubMed: 24533870]
13. Donato F, Costa DN, Yuan Q, et al. Geometric distortion in diffusion-weighted MR imaging of the prostate-contributing factors and strategies for improvement. *Acad Radiol.* 2014; 21:817–823. DOI: 10.1016/j.acra.2014.02.001 [PubMed: 24709379]
14. White NS, Leergaard TB, D’Arceuil H, Bjaalie JG, Dale AM. Probing tissue microstructure with restriction spectrum imaging: histological and theoretical validation. *Hum Brain Mapp.* 2013; 34:327–346. DOI: 10.1002/hbm.21454 [PubMed: 23169482]
15. White NS, McDonald CR, Farid N, et al. Diffusion-weighted imaging in cancer: physical foundations and applications of restriction spectrum imaging. *Cancer Res.* 2014; 74:4638–4652. DOI: 10.1158/0008-5472.CAN-13-3534 [PubMed: 25183788]
16. White N, McDonald C, Farid N, et al. Improved conspicuity and delineation of high-grade primary and metastatic brain tumors using “restriction spectrum imaging”: quantitative comparison with high B-value DWI and ADC. *AJNR Am J Neuroradiol.* 2013; 34:958–964. [PubMed: 23139079]
17. McDonald C, White N, Farid N, et al. Recovery of white matter tracts in regions of peritumoral FLAIR hyperintensity with use of restriction spectrum imaging. *AJNR Am J Neuroradiol.* 2013; 34:1157–1163. DOI: 10.3174/ajnr.A3372 [PubMed: 23275591]
18. Kothari P, White N, Farid N, et al. Longitudinal restriction spectrum imaging is resistant to pseudoresponse in patients with high-grade gliomas treated with bevacizumab. *AJNR Am J Neuroradiol.* 2013; 34:1752–1757. [PubMed: 23578667]
19. Farid N, Almeida-Freitas DB, White NS, et al. Restriction-spectrum imaging of bevacizumab-related necrosis in a patient with GBM. *Front Oncol.* 2013; 30:1–5. DOI: 10.3389/fonc.2013.00258
20. Rakow-Penner R, White N, Parsons J, et al. Novel technique for characterizing prostate cancer utilizing MRI restriction spectrum imaging: proof of principle and initial clinical experience with extraprostatic extension. *Prostate Cancer Prostatic Dis.* 2015; 18:1–5. DOI: 10.1038/pcan.2014.50 [PubMed: 25384337]

21. Liss MA, White NS, Parsons JK, et al. MRI-derived restriction spectrum imaging cellularity index is associated with high grade prostate cancer on radical prostatectomy specimens. *Front Oncol.* 2015; 5:1–8. DOI: 10.3389/fonc.2015.00030 [PubMed: 25667919]
22. Rakow-Penner RA, White NS, Margolis DJ, et al. Prostate diffusion imaging with distortion correction. *Magn Reson Imaging.* 2015; 33:1178–1181. DOI: 10.1016/j.mri.2015.07.006 [PubMed: 26220859]
23. Holland D, Kuperman JM, Dale AM. Efficient correction of inhomogeneous static magnetic field-induced distortion in echo planar imaging. *Neuroimage.* 2010; 50:175–183. DOI: 10.1016/j.neuroimage.2009.11.044 [PubMed: 19944768]
24. Vargas HA, Akin O, Shukla-Dave A, et al. Performance characteristics of MR imaging in the evaluation of clinically low-risk prostate cancer: a prospective study. *Radiology.* 2012; 265:478–487. [PubMed: 22952382]
25. Moore CM, Kasivisvanathan V, Eggener S, et al. Standards of reporting for MRI-targeted biopsy studies (START) of the prostate: recommendations from an International Working Group. *Eur Urol.* 2013; 64:544–552. DOI: 10.1016/j.eururo.2013.03.030 [PubMed: 23537686]
26. Obuchowski N. Nonparametric analysis of clustered ROC curve data. *Biometrics.* 1997; 53:567–578. [PubMed: 9192452]
27. Landis J, Koch G. The measurement of observer agreement for categorical data. *Biometrics.* 1977; 33:159–174. [PubMed: 843571]
28. Tamura C, Shinmoto H, Soga S, et al. Diffusion kurtosis imaging study of prostate cancer: preliminary findings. *J Magn Reson Imaging.* 2014; 40:723–729. DOI: 10.1002/jmri.24379 [PubMed: 24924835]
29. Roethke MC, Kuder TA, Kuru TH, et al. Evaluation of diffusion kurtosis imaging versus standard diffusion imaging for detection and grading of peripheral zone prostate cancer. *Investig Radiol.* 2015; 50:483–489. [PubMed: 25867657]
30. Suo S, Chen X, Wu L, et al. Non-Gaussian water diffusion kurtosis imaging of prostate cancer. *Magn Reson Imaging.* 2014; 32:421–427. DOI: 10.1016/j.mri.2014.01.015 [PubMed: 24602826]
31. Vargas HA, Akin O, Franiel T, et al. Diffusion-weighted endorectal MR imaging at 3 T for prostate cancer: tumor detection and assessment of aggressiveness. *Radiology.* 2011; 259:775–784. [PubMed: 21436085]
32. Cohen MS, Hanley RS, Kurteva T, et al. Comparing the Gleason prostate biopsy and Gleason prostatectomy grading system: the Lahey Clinic Medical Center experience and an international meta-analysis. *Eur Urol.* 2008; 54:371–381. DOI: 10.1016/j.eururo.2008.03.049 [PubMed: 18395322]
33. Kvåle R, Møller B, Wahlqvist R, et al. Concordance between Gleason scores of needle biopsies and radical prostatectomy specimens: a population-based study. *BJU Int.* 2009; 103:1647–1654. DOI: 10.1111/j.1464-410X.2008.08255.x [PubMed: 19154461]
34. Rajinikanth A, Manoharan M, Soloway CT, Civantos FJ, Soloway MS. Trends in Gleason score: concordance between biopsy and prostatectomy over 15 years. *Urology.* 2008; 72:177–182. DOI: 10.1016/j.urology.2007.10.022 [PubMed: 18279938]

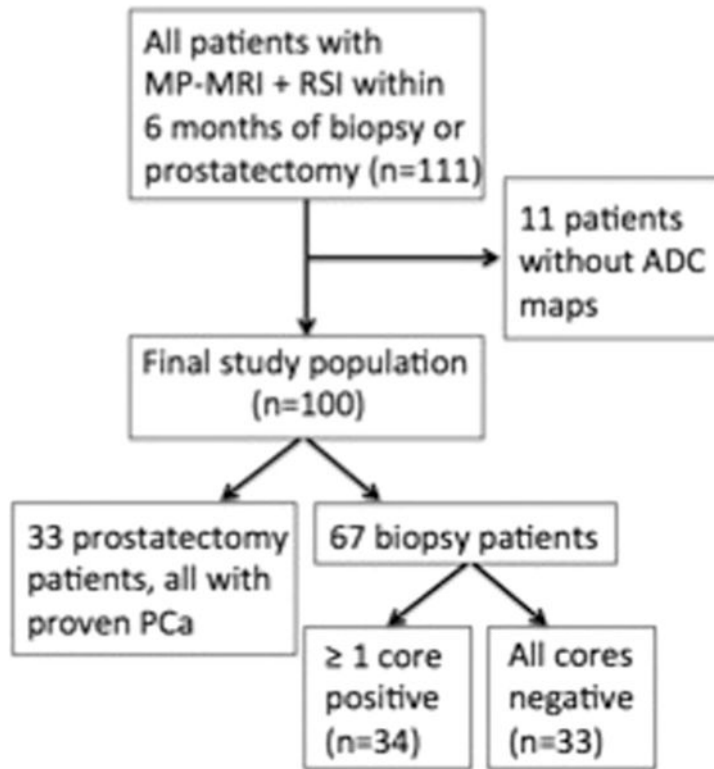


**Fig. 1.** Flowchart summarizes patient selection and tissue standard.

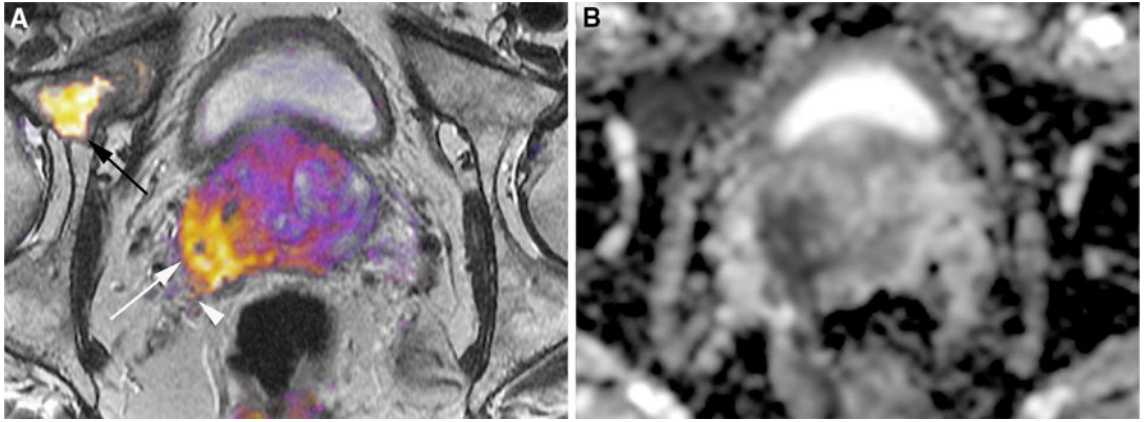


**Fig. 2.** **A** RSI overlaid on T2WI and **B** conventional ADC map in a 64-year-old male with a prostate-specific antigen level of 25.3 ng/mL demonstrates biopsy proven Gleason 4 + 5 involving the right base peripheral zone (*white arrow*) with right-sided extraprostatic extension (*white arrowhead*) and osseous metastatic disease to the right anterior acetabular column (*black arrow*). The ADC map demonstrates marked distortion in the anteroposterior direction, making detection of extraprostatic disease difficult, and demonstrates relatively poor conspicuity of the right acetabular metastasis.

Author Manuscript

Author Manuscript

Author Manuscript

Author Manuscript

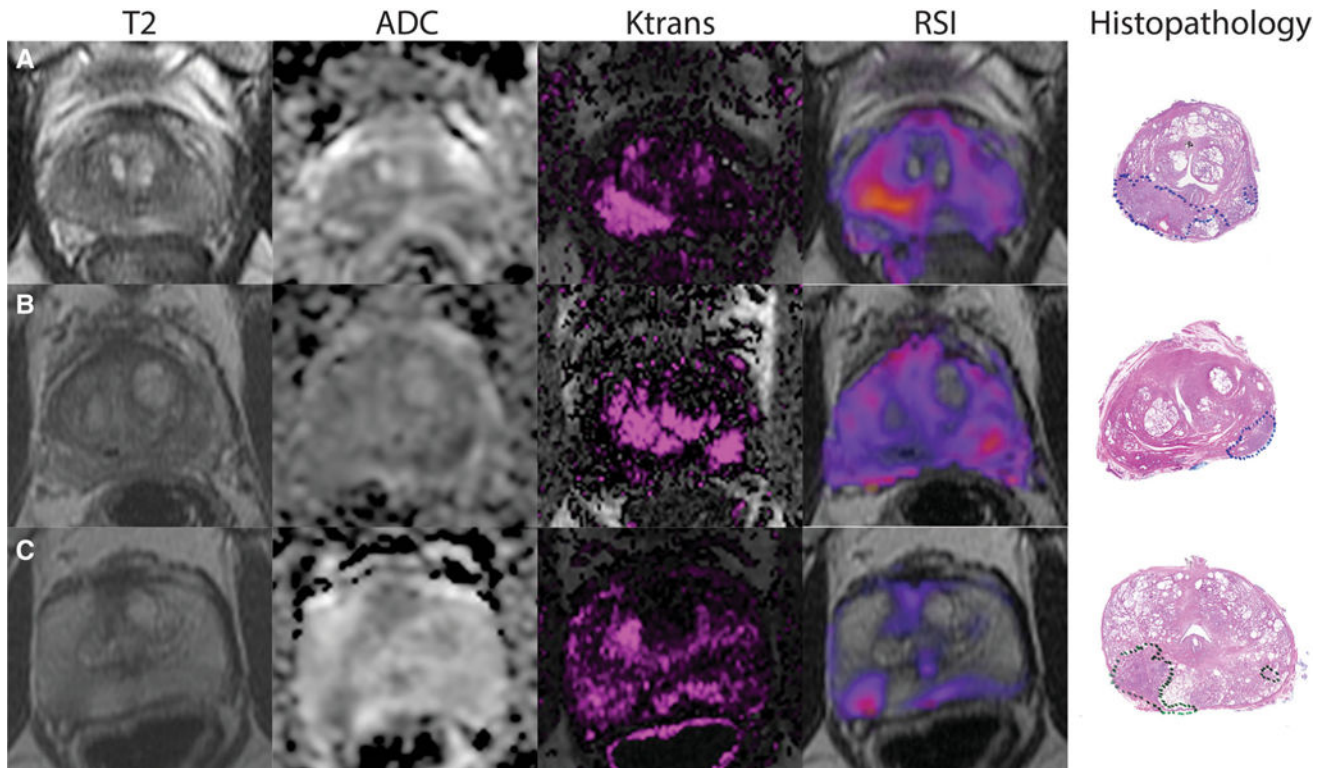


**Fig. 3.** Axial T2WI, ADC map,  $K^{trans}$  maps, and RSI color maps, with subsequent whole mount histopathology in **A** a 58-year-old male with prostate-specific antigen level of 8.2 ng/mL with Gleason Score 4 + 3 disease in the right apex peripheral zone, **B** a 69-year-old male with prostate-specific antigen level of 4.9 ng/mL with Gleason Score 4 + 3 disease in the left base peripheral zone, and **C** a 71-year-old male with prostate-specific antigen level of 6.2 ng/mL with Gleason Score 4 + 3 disease in the right mid peripheral zone. Each case demonstrates increased qualitative conspicuity of prostate cancer on RSI relative to MP-MRI.

**Table 1**

Imaging indications

<b>Indication</b>	<b>Number</b>
Surgical planning	34
Elevated PSA	33
Active surveillance	25
Targeted biopsy planning	11
Abnormal DRE	5
Other <sup>ψ</sup>	3

<sup>ψ</sup> Other causes include perineal pain after biopsy, recurrent prostatitis, and BPH

Author Manuscript

Author Manuscript

Author Manuscript

Author Manuscript

**Table 2**

Imaging parameters

Sequence	Repetition time (ms)	Echo time (ms)	Field of view (mm)	Matrix	Section thickness (mm)	Flip angle (°)	No. of signals acquired
T2WI	4517	90	200–260	384 × 192	3	90	1
DCE	4.5	2.1	200–240	256 × 168	3	30	1
DWI	3750	74	260–360	160 × 160	5	90	8
RSI*	9900	72	200–260	96 × 96	3	90	1

\* RSI is performed at *b*-values of 0, 125, 375, and 1000 s/mm<sup>2</sup> with 6, 6, and 15 directions at each respective non-zero *b*-value

**Table 3**

Patient characteristics

Characteristic	Mean (range)
Age (years)	63.5 (45–80)
PSA (ng/mL)	7.2 (1.1–29.2)
Prostate Volume (mL)	47.3 (16.2–153.8)
Time between MRI and biopsy or prostatectomy (days)	53.4 (5–135)
<hr/>	
Biopsy Gleason score	Number
<hr/>	
Benign	33
3 + 3	15
3 + 4	10
4 + 3	2
4 + 3	7
Prostatectomy Gleason score	
3 + 3	3
3 + 4	9
4 + 3	14
4 + 3	7
Prostatectomy pathologic T stage	
pT2a	2
pT2c	17
pT3a	12
pT3b	2

Author Manuscript

Author Manuscript

Author Manuscript

Author Manuscript



**Table 4**

ROC analysis

Reader	MP-MRI	MP-MRI + RSI	P*	RSI	P $\phi$
Sextant-based analysis					
All PCa					
1	0.63 (0.65)	0.68 (0.70)	<0.001	0.61 (0.60)	0.39
2	0.58 (0.60)	0.64 (0.68)	<0.001	0.63 (0.64)	<0.001
3	0.61 (0.63)	0.66 (0.68)	0.001	0.58 (0.58)	0.08
Combined	0.61 (0.63)	0.66 (0.69)	<0.001	0.61 (0.61)	0.85
High-grade PCa					
1	0.71 (0.69)	0.80 (0.79)	0.01	0.73 (0.69)	0.62
2	0.66 (0.66)	0.75 (0.77)	0.01	0.74 (0.72)	0.03
3	0.72 (0.72)	0.79 (0.78)	0.04	0.66 (0.62)	0.08
Combined	0.70 (0.69)	0.78 (0.78)	<0.001	0.71 (0.68)	0.62
Hemigland-based analysis					
All PCa					
1	0.70 (0.71)	0.71 (0.72)	0.47	0.65 (0.67)	0.13
2	0.63 (0.65)	0.69 (0.71)	<0.001	0.67 (0.69)	0.10
3	0.64 (0.66)	0.69 (0.69)	0.09	0.62 (0.63)	0.48
Combined	0.66 (0.68)	0.70 (0.71)	0.001	0.65 (0.66)	0.64
High-grade PCa					
1	0.82 (0.81)	0.85 (0.84)	0.4	0.82 (0.80)	0.97
2	0.75 (0.75)	0.83 (0.85)	0.1	0.82 (0.79)	0.14
3	0.80 (0.79)	0.85 (0.85)	0.22	0.76 (0.77)	0.45
Combined	0.79 (0.78)	0.85 (0.85)	0.04	0.80 (0.79)	0.77

Data presented are area under the ROC curves (AUC). Data in parentheses represent calculations based on prostatectomy cases alone

\* Represents comparison between MP-MRI and MP-MRI plus RSI AUC

$\phi$  Represents comparison between MP-MRI and RSI AUC

**Table 5**

Inter-reader agreement kappa scores for all possible reader combinations

<b>Reader combination</b>	<b>1,2</b>	<b>2,3</b>	<b>1,3</b>	<b>1,2,3</b>
Protocol				
MP-MRI	0.54	0.52	0.51	0.51
MP-MRI + RSI	0.57	0.53	0.52	0.52
RSI	0.62	0.55	0.55	0.57

Author Manuscript

Author Manuscript

Author Manuscript

Author Manuscript